

Article

Fluid-Structure Interaction Analysis of a Competitive Car during Brake-in-Turn Manoeuvre

Jakub Broniszewski ^{*,†}  and Janusz Ryszard Piechna [†] 

Faculty of Power and Aeronautical Engineering, Warsaw University of Technology, 00-665 Warszawa, Poland; janusz.piechna@pw.edu.pl

* Correspondence: jbroniszewski@meil.pw.edu.pl

† These authors contributed equally to this work.

Abstract: The relationship between the presented work and energy conservation is direct and indirect. Most of the literature related to energy-saving focuses on reducing the aerodynamic drag of cars, which typically leads to the appearance of vehicle motion instabilities at high speeds. Typically, this instability is compensated for by moving aerodynamic body components activated above a certain speed and left in that position until the vehicle speed drops. This change in vehicle configuration results in a significant increase in drag at high velocities. The presented study shows a fully coupled approach to fluid–structure interaction analyses of a car during a high-speed braking-in-turn manoeuvre. The results show how the aerodynamic configuration of a vehicle affects its dynamic behaviour. In this work, we used a novel approach, combining Computational Fluid Dynamics (CFD) analysis with the Multibody Dynamic System. The utilisation of an overset technique allows for car movement in the computational domain. Adding Moving Reference Frame (MRF) to this motion removes all restrictions regarding car trajectory and allows for velocity changes over time. We performed a comparative analysis for two aerodynamic configurations. In the first one, a stationary rear airfoil was in a base position parallel to a trunk generating low drag. No action of the driver was assumed. In the second scenario, brake activation initiates the rotation of the rear airfoil reaching in 0.1 s final position corresponding to maximum aerodynamic downforce generation. Also, no action of the driver was assumed. In the second scenario, the airfoil was moving from the base position up to the point when the whole system approached its maximum downforce. To determine this position, we ran a separated quasi-steady analysis in which the airfoil was rotating slowly to avoid transient effects. The obtained results show the importance of the downforce and load balance on car stability during break-in-turn manoeuvres. They also confirm that the proposed methodology of combining two independent solvers to analyse fluid–structure phenomena is efficient and robust. We captured the aerodynamic details caused by the car’s unsteady movement.

Keywords: vehicle aerodynamics; coupled analysis; car dynamics; FSI; cornering



Citation: Broniszewski, J.; Piechna, J.R. Fluid-Structure Interaction Analysis of a Competitive Car during Brake-in-Turn Manoeuvre. *Energies* **2022**, *15*, 2917. <https://doi.org/10.3390/en15082917>

Academic Editor: João Pombo

Received: 23 February 2022

Accepted: 12 April 2022

Published: 15 April 2022

Publisher’s Note: MDPI stays neutral with regard to jurisdictional claims in published maps and institutional affiliations.



Copyright: © 2022 by the authors. Licensee MDPI, Basel, Switzerland. This article is an open access article distributed under the terms and conditions of the Creative Commons Attribution (CC BY) license (<https://creativecommons.org/licenses/by/4.0/>).

1. Introduction

The relationship between the presented work and energy conservation is direct and indirect. Most publications related to energy conservation focus on reducing the aerodynamic drag of cars. However, typically, the reduction in body aerodynamic drag is simultaneously associated with the generation in body lift force, which causes the appearance of directional instability of the car at high speeds. Therefore, cars are equipped with various types of aerodynamic elements that extend beyond a certain driving speed and are concealed at lower speeds.

With the aerodynamic elements activated, the coefficients of aerodynamic drag are higher than those given in catalogues. Higher drag exists during long trips at high speeds. Aerodynamic drag is proportional to the second power of the car’s velocity.

This work mostly concerns moving aerodynamic elements that are briefly activated when their action is needed. Active aerodynamic elements, used only when necessary, allow for safe long-term driving at high speeds with a low aerodynamic drag for the vehicle. This has a direct relationship with energy savings. This paper presents a modern and unique method of calculating vehicle dynamics and aerodynamics in transient conditions. This makes it possible, using numerical simulations, to obtain information about the required speed of the additional moving aerodynamic elements actuators used during dynamic manoeuvres.

The idea presented in this paper is to increase the average speed of the vehicle without increasing the maximum speed by safely increasing the cornering speed, reducing the frequency of braking before the turn and the subsequent acceleration. At present, especially electrically powered cars suffer from a constant shortage of energy for propulsion, due to the significant energy consumption caused by additional car equipment such as electric air conditioning, ventilation, heating, power steering and braking systems, windshield wipers, headlights and auxiliary lights. Such equipment consumes energy in proportion to driving time rather than speed. Thus, an increase in average speed without an increase in top speed is possible when cornering at a higher safe speed. This reduces the overall travel time, thus reducing the energy consumption of the car's accessories. This is the indirect relationship between the presented work and energy conservation.

Braking-in-turn is one of the most dangerous manoeuvres on the road. This is because even a minor change in downforce distribution can significantly differentiate car behaviour. This was confirmed by an experimental work performed by the BMW team on their Z4 model [1]. They found that more minor changes in the rear lift are necessary to achieve unstable driving conditions at higher speeds. In one of the analysed cases, with the initial velocity $V = 160$ km/h and a curve radius of $R = 400$ m, a change in the rear lift coefficient from 0.13 to 0.165 caused the vehicle to oversteer. When they increased the speed to $V = 200$ km/h and circular track radius to $R = 800$ m, a rear lift of 0.13 caused instability. At the same time, a slight reduction in the rear lift coefficient to 0.12 led to significantly safer driving behaviour. The study presented in [2] highlights the importance of cornering conditions on vehicle aerodynamic performance and the fact that, at present, there is no good way to perform an experiment that will assure the required flow conditions. The authors concluded that numerical simulation could overcome difficulties such as close ground proximity, high blockage ratio and the specific type of motion. However, this analysis has to accommodate the curved flow that occurs within a non-inertial reference frame. The same authors, in a later work [3], developed a new kind of wind tunnel that allows for experimental testing for cornering conditions. It will enable testing in a non-inertia reference frame and accounts for flow curvature in the absence of a static pressure gradient. Josefsson et al. utilised computational fluid dynamics (CFD) to check the impact of cornering conditions on aerodynamic drag [4]. The study covers the steady-state analyses and curvature radius from 100 m to 800 m. The velocity was equal to 90 km/h. The considered vehicle dynamics effects include roll, body slip, and steering angles with rotating wheels calculated according to [5]. The obtained results show that drag for radius 400 m can increase by 10% compared to straight-ahead cases. They also reported that the underbody has a significant impact on the flow. One of the most advanced techniques to simulate cornering using a Large-Eddy Simulation (LES) solver was proposed by Nara et al. [6]. They combined the Arbitrary Lagrangian-Eulerian (ALE) method and the non-inertial reference frame method to analyse acceleration, deceleration and cornering. Predefined car motions included only translational motion and yaw rotational motion data from an actual vehicle running on the Fuji Speed Way circuit. The authors concluded that, besides speed, acceleration and slip angle also affect unsteady pressure field. A separate group of analyses concerns isolated components, such as airfoils, during cornering. Patel et al. analysed the effect of cornering on the aerodynamics of a multi-element wing in the ground effect [7]. The performed study contains CFD validation against wind tunnel test data for straight-line conditions. The authors used a rectangular computational

domain and Rigid Body Motion (RBM) technique to simulate cornering. The results show a slightly reduced downforce for the cornering case compared to the straight-line case. On the other hand, drag increased by around 5% and side force was also produced. A more natural approach to modelling cornering with curved computation domain was presented by Keogh et al. [8]. They analysed the vortex structure of an inverted wing in ground proximity at the steady-state condition. A comparison of the numerical results and wind tunnel data shows that $k-\omega$ SST performs better than $k-\epsilon$. A conducted mesh density study in the range 4.7×10^6 – 13.6×10^6 cells has a limited impact on obtained aerodynamics forces. This untypical conclusion could be caused because the authors analysed an airfoils-only geometry, and the number of cells required to achieve grid convergence is lower than in the so-called coarse mesh. Basso et al. [9] performed a comparative analysis of the Gurney's flap impact mounted on the front wing of the F1 car and the performance characteristics that can also influence the braking process. They used the front part of the entire vehicle to capture the interaction between different components. They concluded that adding this small component increases the downforce by about 24% and has a limited impact on drag force.

To the best of our knowledge, none of the papers describe a methodology for analysing the dynamic behaviour of a car during cornering. We are going even further in this paper, and presenting a novel approach to simulate the brake-in-turn manoeuvre.

2. Description of the Research Problem

The purpose of the simulations was to determine the behaviour of a vehicle during curve travel from the start of the braking process for two traffic scenarios. Scenario one is a vehicle braking with fixed geometry and elastic suspension. Scenario two is activating the rotation of the vehicle's rear wing on the elastic suspension when braking is initiated. Figure 1 shows the problem when analyzed schematically.

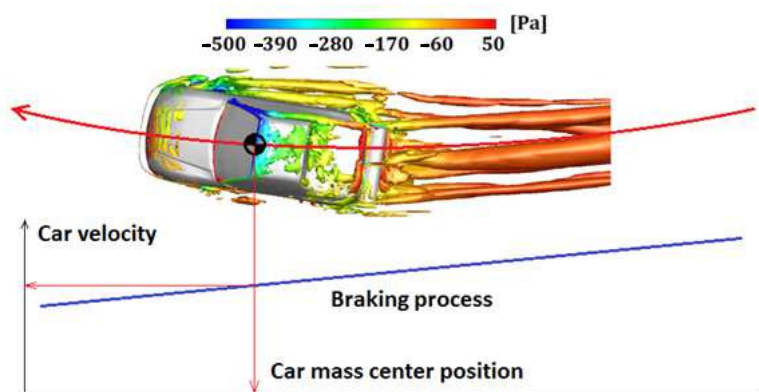


Figure 1. Scheme of the analyzed problem.

Before the initiation of braking on a curve, steady aerodynamic forces and centrifugal force act on the vehicle. At the moment of braking initiation, braking forces appear at the point of contact between the wheels and the road, generating additional inertia forces. The problem is quite computationally challenging, as the vehicle motion speed decreases during braking. The vehicle moves along a curvilinear track and rotates around its centre of mass. This complicated movement is a significant complication in unsteady flow calculations. Additionally, the time-varying aerodynamic and inertial forces significantly influence the local values of the longitudinal and transverse forces occurring at the tyre–road interface and the body's position in relation to the road. To solve this problem, it was necessary to develop a computational model allowing for unsteady calculations of aerodynamic forces acting on a vehicle that changes its position due to inertia and aerodynamic forces. Such a model was developed. The discussed procedure was previously validated by comparison with the results of tunnel tests of self-excited beam oscillations and the vehicle-braking process in track tests [10,11]. Therefore, only numerical simulation results are presented in

this paper to show the influence of the moving aerodynamic elements (moving rear airfoils) on the braking behaviour of the vehicle during cornering. The main problem in vehicle dynamics during cornering is the change in the downforce of the rear and front axle wheels, caused by the inertia forces applied to the vehicle's centre of mass, which is located at a certain distance from the ground. As a result of the inertia forces, the contact between the front wheels and the roadway increases, while the rear wheels lose loading. Under these conditions, during cornering and braking, it is easy for the rear wheels to lose traction and cause the vehicle to rotate.

3. Materials and Methods

A complicated system of inertia forces acting on a car during dynamic passing road corners has a strong influence on the position of the car body in relation to the road and the airflow directions. On the other hand, a change in a car orientation influences the generation of aerodynamic forces. A dynamic balance between inertia and aerodynamic forces requires the simultaneous calculation of these forces by two independent solvers and for information to be exchanged between them at the level of a single integration time step. In a previous work [10], we described and validated a similar approach as applied to the braking process. However, in the current paper, we modified this method. At first, we removed the assumption regarding flow symmetry, and used a complete car body model. We also decided to use a curved computational domain to assure proper flow conditions. Instead of physically moving an object in a calculation domain, we used a Moving Reference Frame (MRF) rotating around the corner center. A summary of the boundary conditions applied to the the background domain faces is presented in Table 1. Curvature radius $R = 800$ m is the same as it was during one of the tests performed by BMW [1].

Table 1. Boundary conditions applied to the CFD background domain.

Region	BC Type	Value
Inlet	Velocity Inlet	0 m/s
Outlet	Pressure Outlet	Ambient
Ground	Wall	no slip, velocity = 0 m/s
Top	Symmetry	-
Sides	Symmetry	-

The main idea behind the analysis concept is to connect CFD and multibody system (MBD) solvers and exchange information. In the proposed solution, we used Ansys Fluent[®] to solve the unsteady flow field and MCS.Adams/Car[®] to perform a dynamic analysis of a full car. Matlab[®] acted as an interface between these two independent solvers. The tools ecosystem utilised Ansys Fluent[®] “As-A-Server” launching option [12]. This option allows for the software to have more than one client and use a COM port to receive requests from a client. In our case, Fluent[®] acts as a COM server, and Matlab[®] is a client. Connection to MCS.Adams/Car[®] was carried with the support of Adams/Controls plugin [13]. This plugin allows one connect Adams[®] model to block the diagram, which were developed in Matlab/Simulink[®].

Matlab/Simulink[®] managed the whole data flow and performed the conversion between coordinate systems. Solvers exchanged data at each time step using the Gauss–Seidel coupling scheme presented in Figure 2. In this approach, the code waits while the partner code proceeds. Figure 3 presents the data flow in the fluid–structure interaction calculation.

We applied the overset mesh technique that is available in Fluent software [14] to allow for the car's movement in the computational domain. Additionally, the car body and wheels were treated as separate bodies that could move independently to allow rotations such as pitch and roll. Airfoils had a relative coordinate system assigned to the car body. This approach simplifies the description of airfoils' movement and requires a definition of relative rotation around one axis. During the calculation, compiled User-Defined-Functions

(UDFs) controlled the movement of all parts and cornering speed. At the end of each time step, UDFs also calculated aerodynamic forces and moments. All subroutines used text files to exchange the data. The selected generalised $k-\omega$ two-equation turbulence model (GEKO) has y^+ -insensitive wall formulation, which allows for the use of the model on meshes of arbitrary y^+ values, as long as the y^+ value lies in the logarithmic layer of the boundary layer [15]. This feature is an essential aspect in our case, because velocity during braking is not constant and, as a consequence, y^+ also changes. The background mesh consists of block-structural mesh to maintain a good mesh quality. Figure 4 presents the main dimensions of the calculation domain and mesh structure in the car proximity, and these are shown in Figure 5.

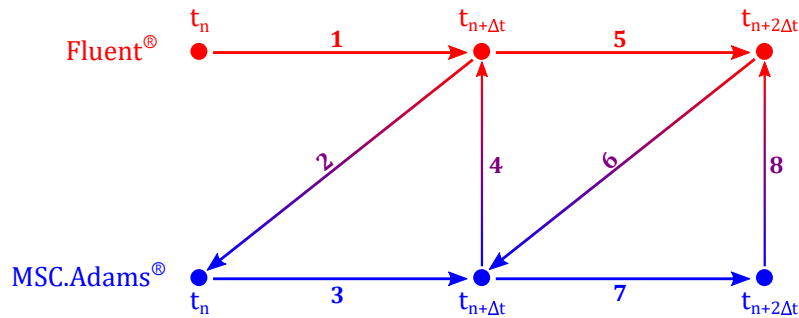


Figure 2. Gauss-Seidel coupling scheme where one code waits while the partner code proceeds.

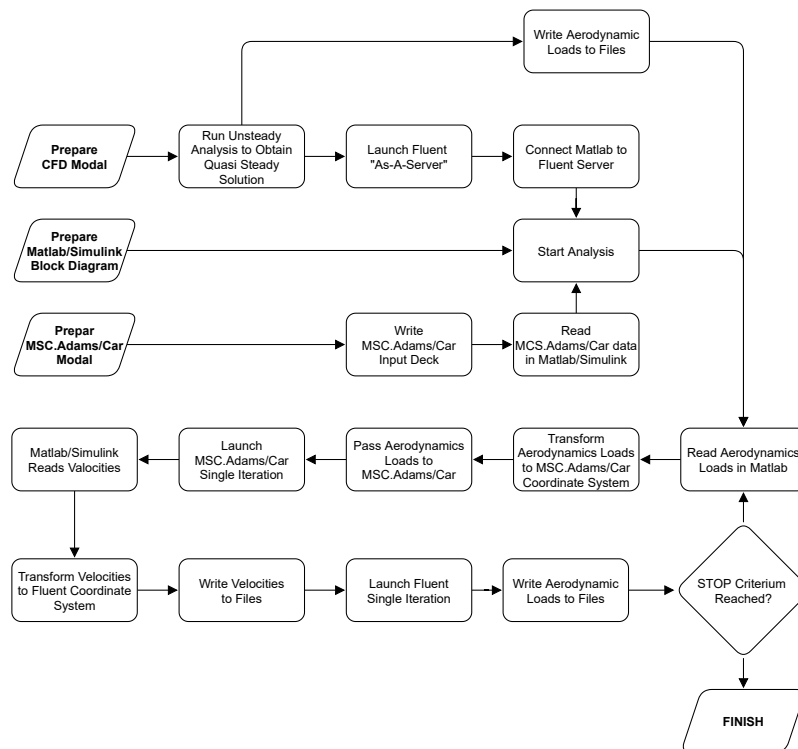


Figure 3. Block diagram which illustrates data flow in fluid-structure interaction process.

The density of the background grid is higher in the proximity of the car body to avoid orphan cells on the overset interfaces. The distribution of the size of the elements on the ground level is presented in Figure 6.

Thanks to Ansys Mosaic-enabled poly-hexcore meshing [16], we have decreased the number of meshing cells for the car body and the rest of the elements compared to the standard triangular or polyhedral meshing technique.

The corresponding full car model was created in MSC.Adams/Car software. Its main components are presented in Figure 7. The model contains features such as a nonlinear damper, which are different for front and rear suspension.

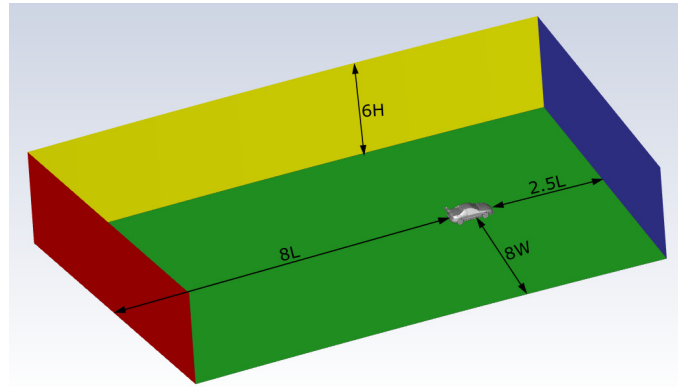


Figure 4. The main dimensions of the calculation domain. L-car length, W-car width, H-car height.

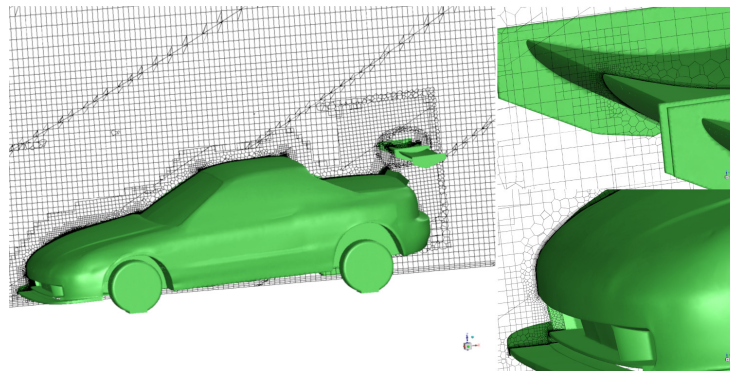


Figure 5. Mesh structure in the car body proximity.

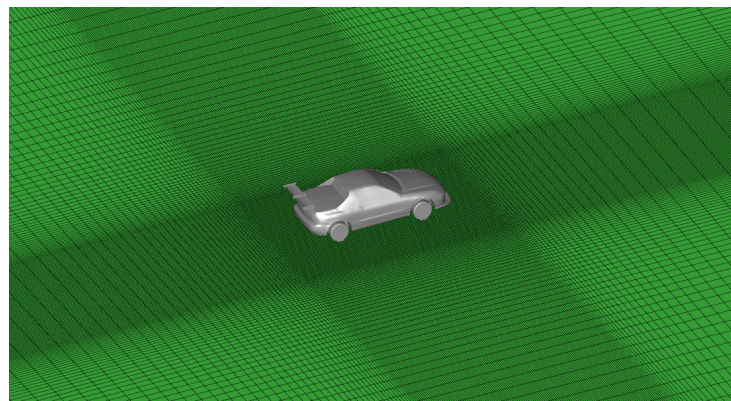


Figure 6. The distribution of the size of the elements on the ground level.

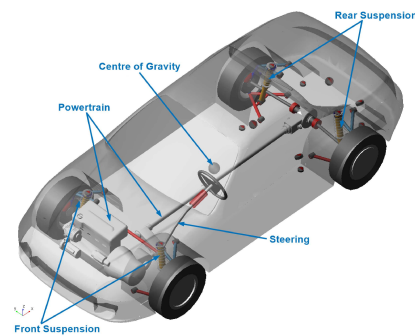


Figure 7. MSC.Adams/Car model used during analysis.

Figure 8 shows the dampers and springs characteristics used during calculation. We fixed the position of a steering wheel during the manoeuvre to allow for a direct comparison of the aerodynamics effect on car stability. Tire modelling utilised Pacejka magic formula [17], and the coefficient of friction between tires and ground was set to 0.72. We estimated mass and momentums of inertia based on the SAE report [18] and the assumed values are presented in Table 2. The details regarding the methodology behind the modelling of a multibody dynamic system are well-described in a book by Blundell and Harty [19].

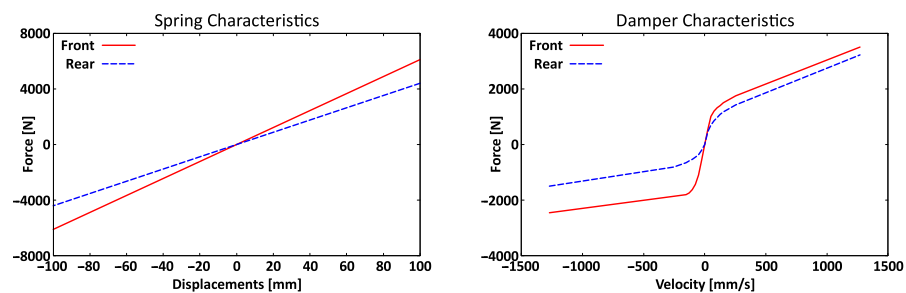


Figure 8. Spring and damper characteristics used during analysis.

Table 2. Mass properties of the car with two passengers used during the analysis.

Parameter	Value	Units
Sprung mass	1300	kg
Pitching moment of inertia	1200	kg·m ²
Yawing moment of inertia	1320	kg·m ²
Rolling moment of inertia	440	kg·m ²

The aeroloads information obtained from a transient CFD analysis is passed onto the dynamic model via block diagram software Matlab/Simulink[®]. The feedback information from the dynamic model, i.e., the car elements velocities, are transferred to the CFD model in the same way. The entire system forms a Fluid–Structure-Interaction solver, allowing one to determine vehicle dynamics behaviour during brake-in-turn manoeuvres.

As the first step in the calculation process, we ran an analysis to determine airfoil rotation angle, which assured the highest downforce of the whole system. During this analysis, boundary conditions were the same as the initial ones for the brake-in-turn calculation. The segmented airfoil rotation was slow enough to avoid transient effects influencing the generated forces. Figure 9 presents the lift vs. airfoil rotation angle characteristic. It can be seen that each of the airfoil components (left and right) achieved maximum downforce at a different airfoil rotation angle. The maximum downforce value for the sum of all components (left and right airfoils and the car body) occurred at an angle of 27°. This value will be used later in the calculation as the final position of the airfoil.

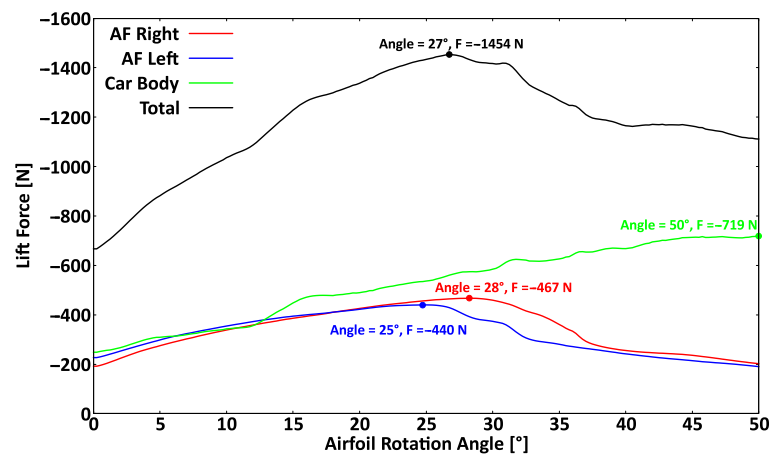


Figure 9. Lift components vs. airfoil rotation angle.

4. Results

4.1. Initial Conditions

As mentioned earlier, the starting point for the analysis is a quasi-steady-state result from a transient analysis performed at a constant cornering speed equal to $V = 160$ km/h (44.4 m/s). Due to the relatively large cornering radius ($R = 800$ m), an asymmetry in the flow at this condition is mainly visible on the upper-back side of the car body. The pressure distribution presented in Figure 10 reveals differences between the inner and outer side of a trunk.

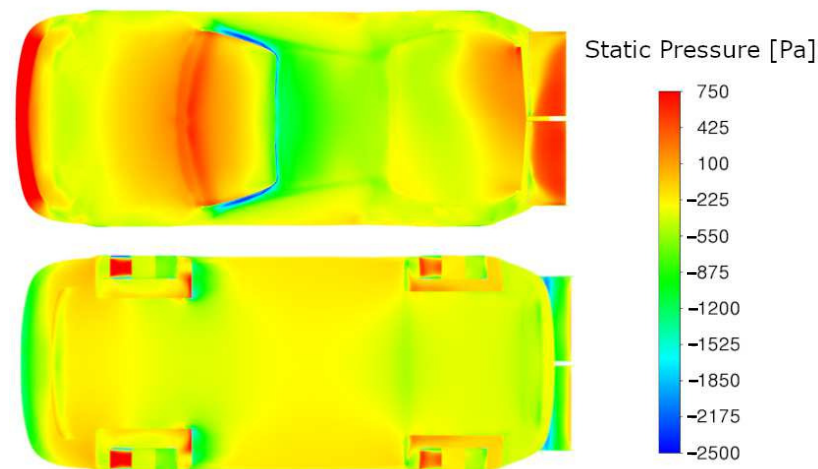


Figure 10. Static pressure on a car body at braking initial condition.

Pressure on the inner side is higher, and the overpressure area is larger. The opposite situation can be observed on the airfoils. The one on the outer side is more loaded. At the same time, pressure on the underbody appears symmetrical over the car's entire length. An explanation for such behaviour can be found in Figure 11.

The streamlines show a large flow separation just after the rear window. The vortex on the inner side is smaller due to the additional flow from the side. This extra flow changes the angle of attack on the inner airfoil and causes separation in the leading edge region.

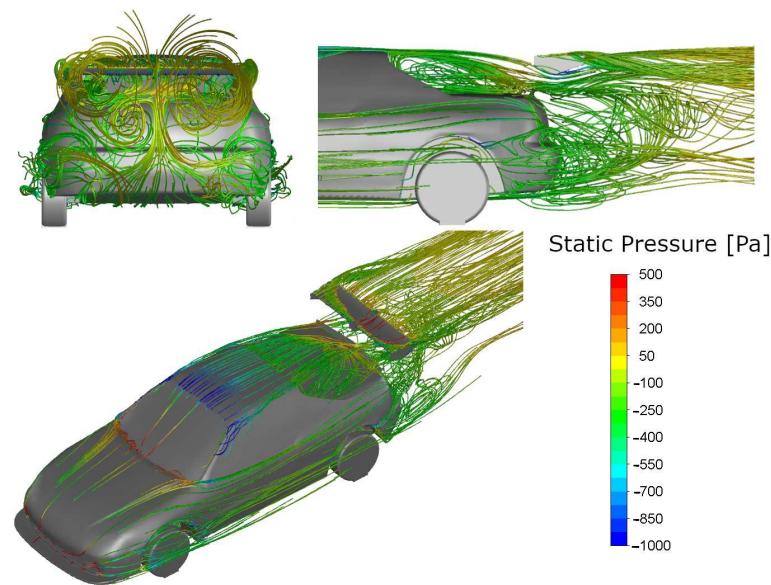


Figure 11. Streamlines at braking initial condition colored with pressure.

4.2. Case with Stationary Airfoils

In the first analysed scenario, rear airfoils were not moving, and they remained in the same position during the whole manoeuvre. In Figure 12, the generated forces correlate with pitch angle (top left), and the maximum downforce is equal to 9.6% of the car weight.

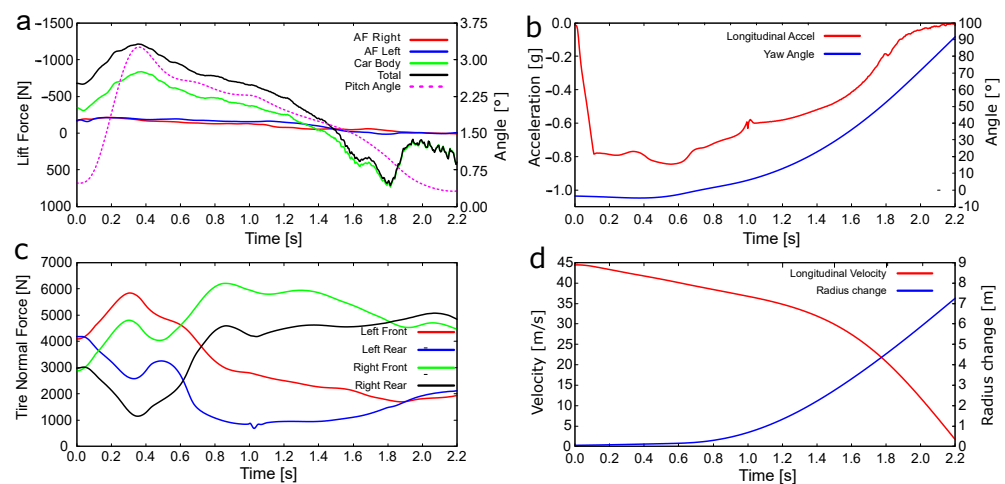


Figure 12. Time history data for the case with stationary airfoils. (a) Lift force and pitch angle vs. time. (b) Acceleration and yaw angle vs. time. (c) Tires normal load vs. time. (d) Velocity and cornering radius change vs. time.

This is caused by the fact that pitch angle impacts clearance between the car body and the ground. The smaller gap generally leads to a higher downforce (negative lift force). On the other hand, a change in pitch angle results from car deceleration (top right). This can be seen a plot with wheels' having a normal load (bottom left). On the bottom right plot, one can notice that longitudinal velocity is almost zero, while we still have a non-zero lift force. Figure 13 helps to clarify the complex movement of the car body.

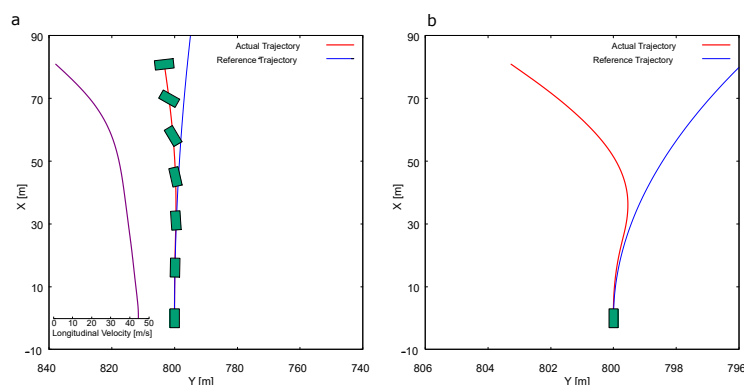


Figure 13. Evolution of the car body orientation during the analysis of the first scenario. (a) Uniform axis scale and velocity profile, (b) Nonuniform scale to highlight character of a deviation.

The x and y axes describe the position of the centre of gravity, and coordinates $(0, 0)$ define the centre of the cornering arc. The blue line represents the desired path for a centre of gravity. The red path shows the actual trajectory. The green boxes indicate the orientation of the car body during the braking manoeuvre. The subplot on the right-hand side shows the same trajectory, with a tighter x -axis scale to highlight the deviation rate from the assumed path. At the beginning of the braking process, the rear wheels are the first ones to lose traction. Without a grip, these wheels slip, the rear axle tends to swing out, and oversteer occurs. The situation changes 0.375 s after the beginning of the braking. The front wheels reach their maximum loading, which is higher than the loading for the rear wheels. As the velocity is large enough, the front wheels, those with traction, lose their grip, because they cannot counteract inertia. This phenomenon is called understeer. This situation leads to significant rotation, and, at a certain point, the longitudinal component of the velocity, measured in the rotating car body coordinate system), reaches a value equal to zero. This does not mean that the velocity magnitude along the path line of the car mass center is also zero, but this was a stop criterion in this particular analysis. It is also important to mention that, at the end of the analysis, the centre of gravity deviated from the ideal trajectory by 7.26 m. On most race tracks, this will mean that the car will fall off the road.

In the time history data in Figure 12 (top right corner), one can notice two points that correspond with the extreme value of lift force. The first one, at time 0.345 s, defines the maximum downforce, and the second, at 1.81 s, is the maximum lift force. We will now take a closer look at the flow structure for these two data points. First, we will look at the pressure distribution on the car's surface to understand where the downforce is generated.

Figure 14 has a significantly lower pressure on the front part of an underbody, and higher pressure on the bonnet, compared to the initial braking condition. The differences in the rear part of the car were much more minor. We can find the reason for this in Figure 15, which presents the velocity magnitude at two sections, each one in the middle of the left and right airfoils.

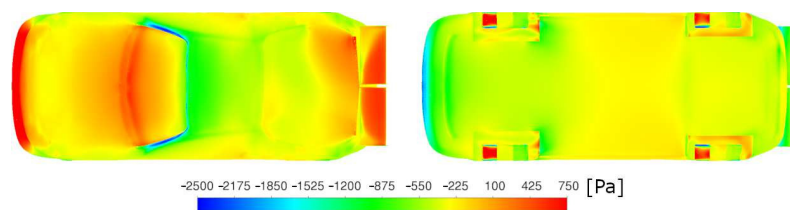


Figure 14. Static pressure on a car body at maximum downforce condition.

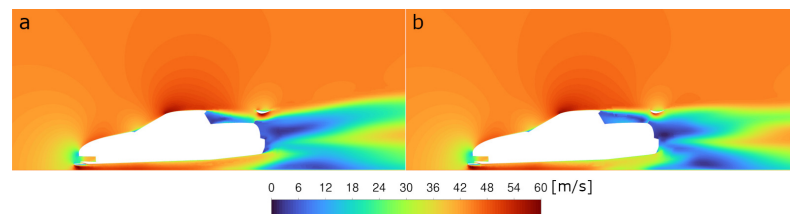


Figure 15. Velocity magnitude in two sections at the maximum downforce condition for the case with stationary airfoil: (a) in the middle of right airfoil; (b) in the middle of left airfoil.

One can notice a visible change in pitch angle, which results in a smaller clearance at the front of the car. As the amount of air directed to the underbody is almost constant, this leads to a higher velocity. Due to the pitch angle, the speed decreases in the rear part of the underbody, and the pressure is comparable to the pressure in the initial braking condition. The streamlines visualisation presented in Figure 16 reveals a change in the vortex structure behind the car. At maximum downforce conditions, the separation bubble at the rear bumper merges with the vortices generated on the airfoils. The potential reason for this is the high-energy air coming from the underbody. With the pitch angle caused by deceleration, the shape of the underbody acts as a diffuser.

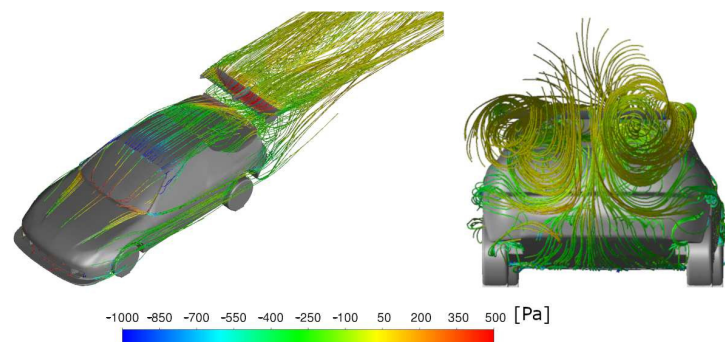


Figure 16. Streamlines at the maximum downforce condition coloured with static pressure.

The maximum lift force, equal to 6.9% of the car weight, occurs when the car yaw angle is 53.4° . The streamlines presented in Figure 17 illustrate the flow structure.

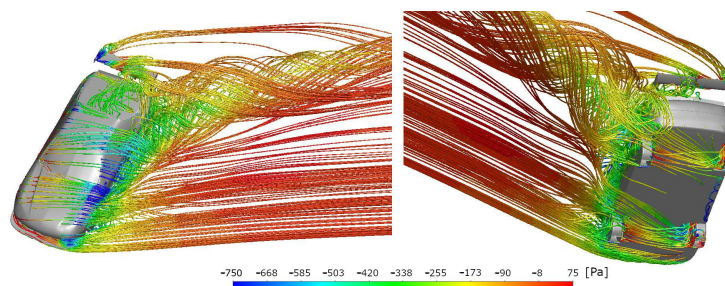


Figure 17. Streamlines at the maximum lift condition coloured with static pressure for the case with stationary airfoil.

One can see that the flow direction is mainly from the side. Designers do not optimize the cars for this condition, resulting in separation on the leeward side. The large vortex is generated over the entire car length, and detaches at the rear bumper region. Due to the flow direction and presence of the endplates, the flow on the airfoils is almost entirely separated. Another confirmation of this observation is visible in Figure 18 (right-hand side), which shows the isosurface of q -criterion coloured with static pressure.

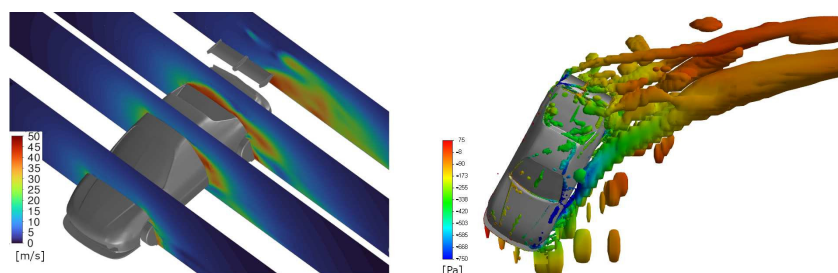


Figure 18. Velocity magnitude (left-hand side) and q-criterion coloured with static pressure (right hand side) at maximum lift condition.

The vortex structure is visible, and indicates the movement direction. On the left-hand side of the same illustration, one can observe the velocity magnitude in the planes perpendicular to the car. On these planes, one can see the growth in the vortex structure from the front to the rear part of the car, indicated by the regions with high velocity.

All the previous observations resulted in the pressure distribution shown in Figure 19. The high pressure on the windward side of the car results from direct flow impingement. There are no significant over-pressure areas on the top of the car body, contributing to the downforce. At the same time, the underpressure regions on the underbody are relatively small. Combining these factors explains the large lift force at this flow condition.

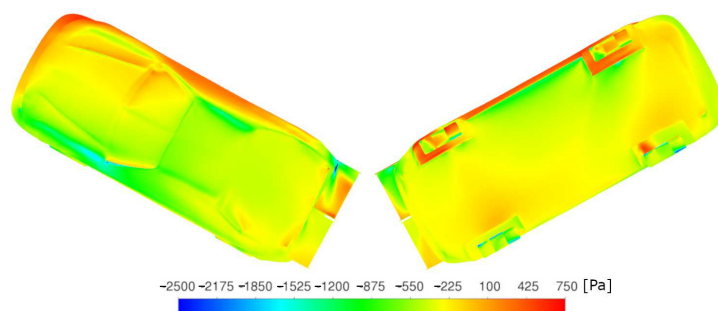


Figure 19. Static pressure on a car body at maximum lift condition for the case with stationary airfoil.

4.3. Case with Moving Airfoils

The second scenario involves airfoils rotations. As we stated in the introduction section, the final rotation angle of 27° corresponds to the maximum downforce for the entire system at quasi-steady conditions. We assumed that both airfoils rotate simultaneously, and it takes 0.1 s to reach the final position. Independent airfoil movement is an opportunity for further optimization, and we did not cover this aspect in this paper. In Figure 20 (top left), airfoil rotation causes a rapid downforce increase, which is visible in the airfoil characteristics.

The maximum total downforce is equal to 14% of the sprung mass of the car. One can notice that loading on the airfoils increased compared to the first scenario due to a change in the angle. At the same time, loading on the car body also increased. Such behaviour is evidence of aerodynamic interaction between the components in the system. Here, we can conclude that the superposition of forces calculated on the isolated components leads to inaccurate results. The plot also indicates that the car reaches maximum pitch angle later than its maximum downforce. By adding data to the second subplot (bottom left), one can notice a correlation between total lift force and normal load on the front wheels. The second correlation is between pitch angle and normal load on the rear right wheel. In the analyzed scenarios, we assumed the right turn. According to this expectation, the left wheels are more loaded than the right ones. A total of 1.5 s after braking beginning, the process stabilizes, and the car starts to move almost linearly. The forces change proportionally to the square of velocity magnitude, and the yaw angle (top right plot) changes linearly over time. One can make a similar observation based on the bottom right plot, where the velocity changes linearly with time, like an instantaneous cornering radius. The evolution

of the car body orientation presented in Figure 21 reveals that the additional downforce that comes from changing the angle of the rear airfoil results in a stable car movement.

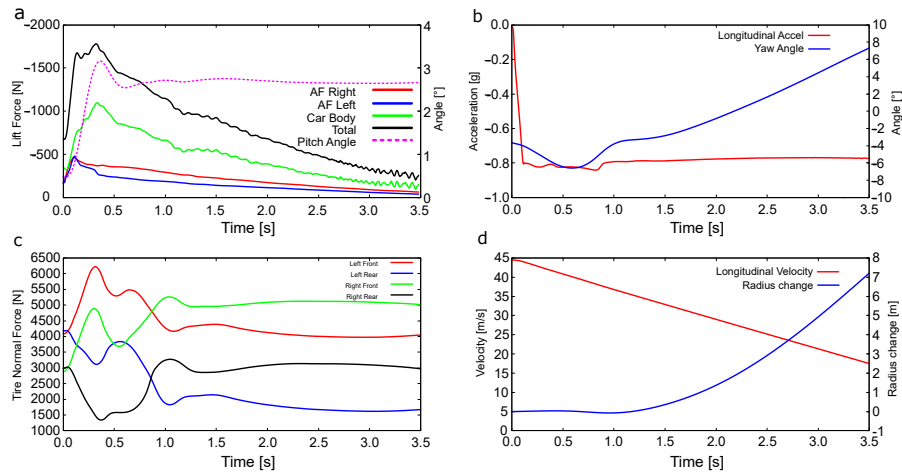


Figure 20. Time history data for the case with moving airfoils. (a) Lift force and pitch angle vs. time. (b) Acceleration and yaw angle vs. time. (c) Tires normal load vs. time. (d) Velocity and cornering radius change vs. time.

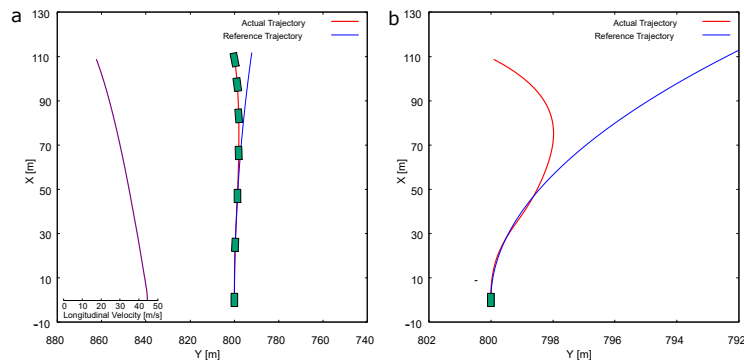


Figure 21. Evolution of the car body orientation during the analysis of the second scenario. (a) Uniform axis scale and velocity profile, (b) Nonuniform scale to highlight character of a deviation.

During the analysis, the steering wheel remains in the same position. A driver does not oppose the car’s rotation by turning the steering wheel. The vehicle does not deviate uncontrollably from the assumed trajectory, even with this restriction.

Pressure contours in Figure 22 presented for the time point with maximum downforce for the entire system show how the airfoils’ movement impacts load distribution.

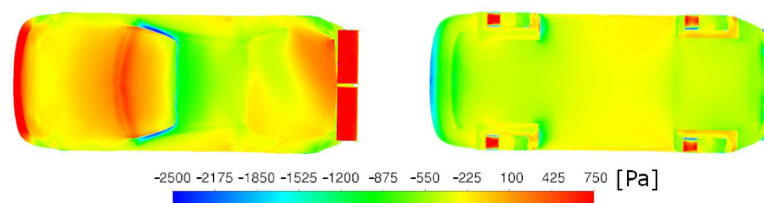


Figure 22. Static pressure on a car body at maximum lift condition.

It is visible that pressure increases on the part of the trunk compared to the stationary airfoils case, and the airfoils are also more loaded. Figure 23 presents areas with overpressure on the top surface of the car and underpressure on the underbody.

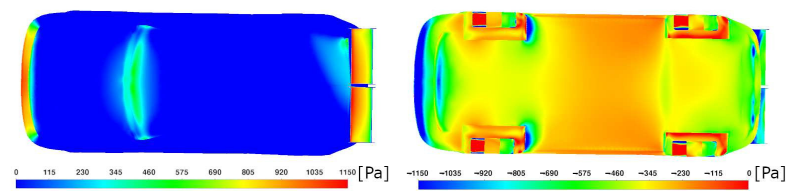


Figure 23. Static over-pressure on a top of the car body and under-pressure on the underbody of the car body at maximum downforce conditions.

The data reveal the regions that are responsible for the downforce generation. One can see that a large amount of downforce comes from the underbody. The conclusion is that controlling the clearance between the car and the ground plays a crucial role in downforce generation. Flow asymmetry is visible in Figure 24, which presents overpressure on the concave side and underpressure on the convex side of the airfoils.

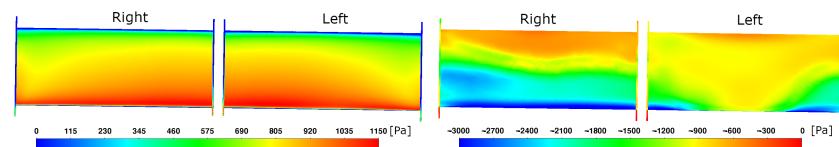


Figure 24. Static over-pressure on a concave side of the airfoils and under-pressure on a convex side of the airfoils at maximum downforce condition.

Pressure distribution suggests that the separation on the left airfoil segment is much bigger than that on the right one. One can find further evidence of this fact by observing the velocity distribution presented in Figure 25.

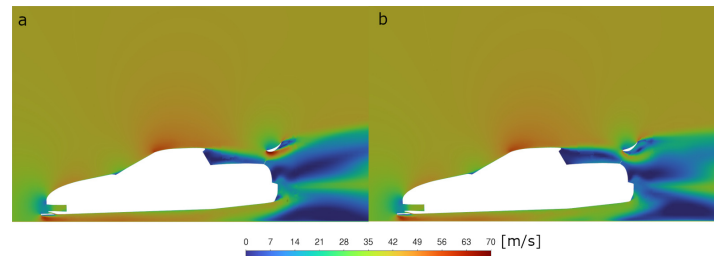


Figure 25. Velocity magnitude in two sections at the maximum downforce condition: (a) in the middle of right airfoil; (b) in the middle of left airfoil.

A separation bubble manifests as a low-velocity area just next to the left airfoil. The final confirmation of this separation can be found in Figure 26 where the streamlines expose the flow structure and aerodynamic interaction between the trunk and airfoils flow.

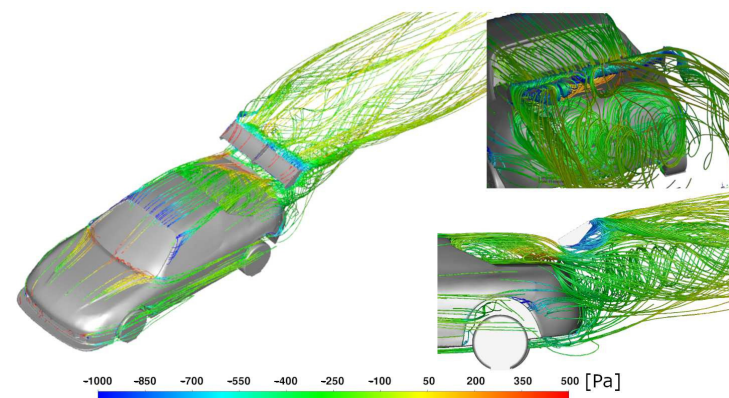


Figure 26. Streamlines at the maximum downforce condition coloured with static pressure.

4.4. Comparison of Two Scenarios

Figure 27 shows the variation in the aerodynamic lift force for the car with the rear wing set at different angles of attack in a cornering configuration. The lift forces are shown separately for each component to show the strong aerodynamic interaction between the car body and the wing segments. The rear wing elements set at a large angle of attack work in the aerodynamic drag generation mode with strong flow separation. Acting on the body causes an increase in pressure on the rear part of the body, generating additional downforce. The presented comparisons highlight the significant impact of the interaction between the body and the segmented rear wing on the flow structures.

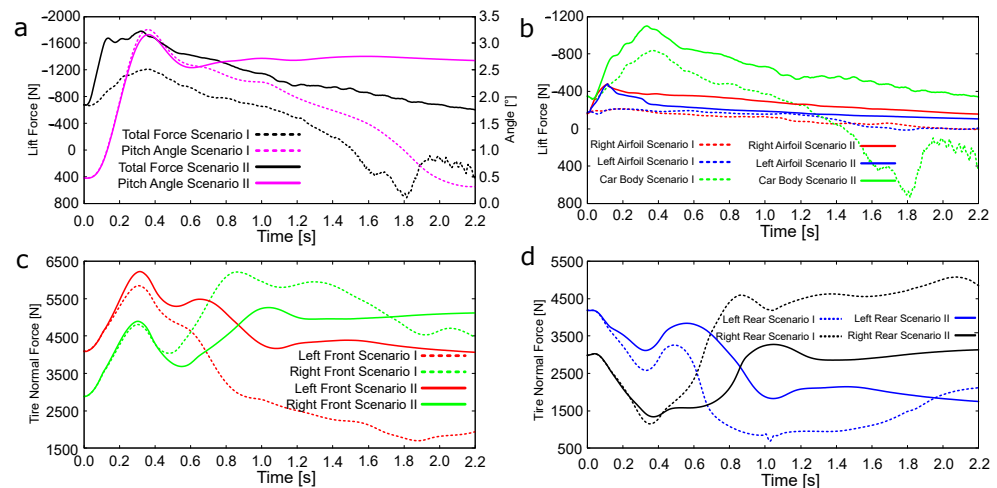


Figure 27. Lift force and tires' normal load comparison for two analyzed scenarios. Scenario I refers to the case with non-moving airfoil and Scenario II refers to case with airfoil rotation. (a) Total lift force and pitch angle vs. time. (b) Components lift force vs. time. (c) Front tires normal load vs. time. (d) Rear tires normal load vs. time.

5. Conclusions

A complicated but effective algorithm has been proposed to combine the CFD solver and car dynamics' solver to analyze the vehicle's transient braking process during cornering. To simulate the body motion and the rear wing rotation, we used the method of superimposed meshes (overset mesh). A Moving Reference Frame method allows for the time-varying flow velocity resulting from the vehicle braking process to be taken into account. The combination of these methods allows for the complicated time-varying flow around the car to be realized.

It seems that the method developed to conduct simulations of transient vehicle motion has no limitations. The results obtained during calculation can also be used to determine the reaction time, speed and force of the actuators required to effectively move aerodynamic features. This knowledge will allow one to realize complex vehicle manoeuvre scenarios.

The total loss of control over vehicle motion during the braking process on a curve in a fixed aerodynamic configuration, and the control retention in a case with an active change in the rear wing inclination, has been demonstrated. The presented data highlight the significant and positive impact of the interaction of flow structures, the body and the segmented rear wing in active state. Car motion was stabilized in two ways: by increasing the aerodynamic downforce on the vehicle's rear wheels, counteracting slipping, and by an additional aerodynamic drag force applied behind the vehicle's centre of mass. The proposed aerodynamic method of actively counteracting the loss of control of vehicle motion during corner braking appears to be more effective and safer at a high initial vehicle speed than a mechanical system based on individual vehicle wheel braking changes.

Author Contributions: Conceptualization, J.B.; Formal analysis, J.B.; Methodology, J.B. and J.R.P.; Supervision, J.R.P.; Visualization, J.B.; Writing—original draft, J.B. and J.R.P. All authors have read and agreed to the published version of the manuscript.

Funding: This project was partially funded by the National Center for Research and Development (Narodowe Centrum Badań i Rozwoju), grant number PBS3/B6/34/2015, “The active system of car body oscillation damping”.

Institutional Review Board Statement: Not applicable.

Informed Consent Statement: Not applicable.

Data Availability Statement: Not applicable.

Conflicts of Interest: The authors declare no conflict of interest.

References

1. Winkelmann, H. Aerodynamics of the new BMW Z4. In Proceedings of the 4th MIRA International Vehicle Aerodynamics Conference, Gaydon, UK, 25–26 October 2006; MIRA: Warwick, Australia, 2002.
2. Keogh, J.; Barber, T.; Diasinos, S.; Doig, G. Techniques for Aerodynamic Analysis of Cornering Vehicles. In Proceedings of the 18th Asia Pacific Automotive Engineering Conference Proceedings, Melbourne, Australia, 10 March 2015. [\[CrossRef\]](#)
3. Keogh, J.M.; Barber, T.; Diasinos, S.; Doig, G. A New Type of Wind Tunnel for the Evaluation of Curved Motion. In Proceedings of the 54th AIAA Aerospace Sciences Meeting, San Diego, CA, USA, 4–8 January 2016.
4. Josefsson, E.; Hagvall, R.; Urquhart, M.; Sebben, S. Numerical Analysis of Aerodynamic Impact on Passenger Vehicles during Cornering. In Proceedings of the CO₂ Reduction for Transportation Systems Conference, Turin, Italy, 21–22 June 2018; SAE International: Warrendale, PA, USA, 2018.
5. Jacobson, B. Vehicle Dynamics Compendium for Course MMF062. 2015. Available online: https://publications.lib.chalmers.se/records/fulltext/225751/local_225751.pdf (accessed on 18 February 2022).
6. Nara, K.; Tsubokura, M.; Ikeda, J. A Numerical Analysis of Unsteady Aerodynamics of Formula Car During Dynamic Cornering Motion. In Proceedings of the 32nd AIAA Applied Aerodynamics Conference, Atlanta, GA, USA, 16–20 June 2014.
7. Patel, D.; Garmory, A.; Passmore, M. The Effect of Cornering on the Aerodynamics of a Multi-Element Wing in Ground Effect. *Fluids* **2021**, *6*, 3. [\[CrossRef\]](#)
8. Keogh, J.; Doig, G.; Diasinos, S.; Barber, T. The influence of cornering on the vortical wake structures of an inverted wing. *Proc. Inst. Mech. Eng. Part D J. Automob. Eng.* **2015**, *229*, 1817–1829. [\[CrossRef\]](#)
9. Basso, M.; Cravero, C.; Marsano, D. Aerodynamic Effect of the Gurney Flap on the Front Wing of a F1 Car and Flow Interactions with Car Components. *Energies* **2021**, *14*, 2059. [\[CrossRef\]](#)
10. Broniszewski, J.; Piechna, J. A fully coupled analysis of unsteady aerodynamics impact on vehicle dynamics during braking. *Eng. Appl. Comput. Fluid Mech.* **2019**, *13*, 623–641. [\[CrossRef\]](#)
11. Piechna, J.R.; Kurec, K.; Broniszewski, J.; Remer, M.; Piechna, A.; Kamieniecki, K.; Bibik, P. Influence of the Car Movable Aerodynamic Elements on Fast Road Car Cornering. *Energies* **2022**, *15*, 689. [\[CrossRef\]](#)
12. ANSYS, Inc. *ANSYS Fluent as a Server User’s Guide (2021R1)*; ANSYS, Inc.: Cannonsburg, PA, USA, 2020.
13. Software, M. Getting Started Using Adams/Controls—Adams 2012.1.2. 2014. Available online: <https://www.atozrealtors.com/simcompanion/infocenter/index?page=content&id=DOC10042&actp=LIST&showDraft=false> (accessed on 18 February 2022).
14. Ramakrishnan, S.; Scheidegger, T. Overset Meshing in ANSYS Fluent. In Proceedings of the 13th Symposium on Overset Composite Grids and Solution Technology, Mukilteo, WA, USA, 17–20 October 2016.
15. Menter, F.R.; Lechner, A.M. *Best Practice: Generalized k- ω Two-Equation Turbulence Model in ANSYS CFD (GEKO)*; ANSYS Technical Report; ANSYS Inc.: Canonsburg, PA, USA, 2021.
16. Zore, K.; Sasanapuri, B.; Parkhi, G.; Varghese, A. Ansys mosaic poly-hexcore mesh for high-lift aircraft configuration. In Proceedings of the 21st AeSI Annual CFD Symposium, Bangalore, India, 8–9 August 2019.
17. Pacejka, H. *Tyre and Vehicle Dynamics*; Butterworth Heinemann: Oxford, UK, 2006.
18. Heydinger, G.J.; Bixel, R.A.; Garrott, W.R.; Pyne, M.; Howe, J.G.; Guenther, D.A. *Measured Vehicle Inertial Parameters-NHTSA’s Data through November 1998*; SAE Technical Paper; SAE International: Warrendale, PA, USA, 1999. Available online: <https://www.nhtsa.gov/DOT/NHTSA/NRD/Multimedia/PDFs/VRTC/ca/capubs/sae1999-01-1336.pdf> (accessed on 11 January 2022).
19. Blundell, M.; Harty, D. *The Multibody Systems Approach to Vehicle Dynamics*, 2nd ed.; Butterworth-Heinemann: Oxford, UK, 2015. [\[CrossRef\]](#)